DOI: 10.1002/ ((please add manuscript number))

Article type: Research Article

Adhesive hydrogel patch-mediated combination drug therapy induces regenerative wound healing through reconstruction of regenerative microenvironment

Soung-Hoon Lee[†], *Soohwan An*[†], *Yeong Chan Ryu, Seol Hwa Seo, Sohyun Park, Mi Jeong Lee, Seung-Woo Cho, and Kang-Yell Choi**

Dr. S.-H. Lee, Dr. S. An, Dr. Y. C. Ryu, Dr. S. H. Seo, S. Park, M. J. Lee, Prof. S.-W. Cho, Prof. K.-Y. Choi

Department of Biotechnology

Yonsei University

Seoul 03722, Republic of Korea

E-mail: kychoi@yonsei.ac.kr

Dr. S.-H. Lee, S. Park, Prof. K.-Y. Choi

CK Regeon Inc.

Seoul 03722, Republic of Korea

[†]These authors contributed equally to this work

[*]Corresponding authors

Keywords: Skin regeneration, Regenerative wound healing, Wnt/β-catenin pathway, Adhesive hydrogel patch, Combination drug therapy

Abstract

Regenerative wound healing involves the complete regeneration and scarless healing of wounded skin as observed in fetal skin. Multiple features of regenerative wound healing have been well studied; however, the practical application of pro-regenerative materials to recapitulate the regenerative wound healing in adult skins has not yet been achieved. In this study, we identified that our novel pro-regenerative material, pyrogallol-functionalized hyaluronic acid (HA-PG) patches in combination with protein transduction domain-fused Dishevelled (Dvl)-binding motif (PTD-DBM), a peptide inhibiting the CXXC-type zinc finger protein 5 (CXXC5)-Dvl interaction, promoted regenerative wound healing in mice. The HA-PG patches loaded with this competitor peptide and valproic acid (VPA), a glycogen synthase kinase 3β inhibitor, significantly inhibited scar formation during wound healing. The HA-PG patches with PTD-DBM and/or VPA inhibited the expression of differentiated cell markers such as α-smooth muscle actin while inducing the expression of stem cell markers such as CD105 and Nestin. Moreover, Collagen III, an important factor for regenerative healing, was critically induced by the HA-PG patches with PTD-DBM and/or VPA, as also seen in VPA-treated *Cxxc5*$^{-/-}$ mouse fibroblasts. Overall, these findings suggest that our novel regeneration-promoting material can be utilized as a potential therapeutic agent to promote both wound healing and scar attenuation.

1. Introduction

Regenerative wound healing refers to the formation of normal, scar-free skin tissue after injury, and there are two primary models of regenerative healing.[1-3] First, human fetal skin can regenerate without scar formation after wounding, and fetal skin wound healing exhibits a different healing pattern from adult wound healing where scars remain.[3, 4] In fetal wounds, stem cells are more present than myofibroblasts, and inflammatory cells are significantly reduced compared with adult wounds.[5] In addition, fetal wounds are characterized by a high ratio of Collagen III/Collagen I, and the high expression of Collagen III plays a crucial role in the regenerative healing of fetal wounds.[4] As another model, the African spiny mouse (*Acomys cahirinus*) exhibits a scarless regenerative wound healing pattern during wound healing.[1] F4/80-positive macrophages and many proinflammatory cytokines are almost absent, and the levels of fibrotic collagens are very low in *Acomys cahirinus* compared with *Mus musculus*.[6] Given the characteristics of the two models for regenerative healing, the use of biomaterials to produce pro-regenerative signals that induce

specific cell types and extracellular matrix (ECM) composition is essential for recapitulating regenerative healing in adult wounds.[3]

Wnt/β-catenin signaling pathway plays pivotal roles in skin regeneration.[7-10] The Wnt/β-catenin pathway promotes cutaneous wound healing,[11] and CXXC-type zinc finger protein 5 (CXXC5), a negative regulator of this pathway, inhibits wound healing in human and mouse skins.[12] Protein transduction domain-fused Dishevelled (Dvl)-binding motif (PTD-DBM), a peptide blocking CXXC5-Dvl interactions, activates the Wnt/β-catenin pathway by inhibiting CXXC5 function and accelerates cutaneous wound healing.[12]

Moreover, the Wnt/β-catenin pathway is highly involved in regenerative healing.[3, 13] *CD44*, a Wnt/β-catenin pathway target gene, is a major receptor for hyaluronic acid (HA), one of the ECM components crucial for regenerative healing.[14, 15] C-X-C chemokine receptor type-4 (CXCR4), another Wnt/β-catenin pathway target gene involved in tissue regeneration, is a chemokine receptor responsible for mesenchymal stem cell (MSC) migration and is strongly expressed in MSCs.[3, 16, 17] Furthermore, several ligands of the Wnt/β-catenin pathway, including Wnt7a and Wnt9, are significantly up-regulated in *Acomys cahirinus* compared with the levels in *Mus musculus*.[13] Despite the significance of the Wnt/β-catenin pathway in the context of regeneration, pro-regenerative materials targeting this pathway have yet to be developed. Importantly, the pro-regenerative materials should be applied to wound sites in a localized and controlled manner, as the Wnt/β-catenin pathway is related to several biological pathways in many different tissues.[18, 19] Moreover, the wound sites are typically in contact with body fluids and blood, thus making it difficult to achieve effective and prolonged delivery of therapeutic materials.[20] Based on this, HA-based bio-adhesive biomaterials are promising candidates for the prolonged and localized delivery of agents

activating the Wnt/β-catenin pathway when applied to a wound site to induce the regenerative wound healing. Thus, we developed and used an ascidian-inspired pyrogallol (PG)-functionalized HA (HA-PG) patch as a drug delivery sytem for local and sustained delivery of pro-regenerative materials to the wounds. Due to the superior affinity of the PG group for various substances, the hydrogel patch can facilely encapsulate multiple drugs that synergistically work for skin regeneration.[21] Therefore, the multi-drug delivery can be achieved easily and efficiently by just placing the patch onto the wound site without any complex procedures or methods. Furthermore, the HA-PG patch inspired by marine ascidian can be self-crosslinked due to the autoxidative properties of the PG group and adhered onto the wound site, where body fluids exist, thereby enabling local and sustained drug delivery.[22, 23] In addition, HA is one of the ECM components constituting skin tissue, and is a highly biocompatible biopolymer.[24] Synthetically, the HA-PG patch would not only show superior skin regeneration capabilities as an off-the-shelf drug delivery system and wound dressing with excellent biocompatibility but also provide the potential for clinical translation and commercialization.

We have found that the blockade of CXXC5 function by PTD-DBM provides a safe approach for activation of the regenerative Wnt/β-catenin pathway.[8] Therefore, we evaluated the therapeutic effect of an HA-PG patch combined with valproic acid (VPA), a glycogen synthase kinase 3β (GSK3β) inhibitor,[10] and/or PTD-DBM on scar formation in the cutaneous wounds (**Figure 1**). Here, we found that the application of HA-PG patches combined with PTD-DBM and VPA onto wounds greatly attenuated scar formation. Stem cell expression and the production of reactive oxygen species (ROS) were also measured in the wounds to determine the effect on regenerative wound healing. In addition, expression of CXCR4, the activator of tissue regeneration and target of the Wnt/β-catenin pathway,[16, 17] was identified in the wounds regenerated by HA-PG+PTD-

DBM+VPA. Finally, we examined several markers of healing in *Cxxc5*$^{+/+}$ and *Cxxc5*$^{-/-}$ mouse fibroblasts to elucidate the mechanism underlying regenerative wound healing facilitated by inhibition of Cxxc5 function.

The treatment with HA-PG patches loaded with PTD-DBM and VPA provides a novel and effective therapeutic approach to regenerative wound healing while minimizing scar formation. In addition, this biomaterial is highly convenient to facilitate wound healing by a single application due to the efficient and sustained delivery of substances loaded into the patches.

2. Results

2.1. Self-crosslinking and tissue-adhesiveness of the HA-PG patches

The HA-PG conjugate was synthesized by conjugating the PG group to HA via carbodiimide chemistry (**Figure 2**a). The presence of a peak indicating aromatic protons of PG groups (~6.4 ppm) in the ^{1}H-nuclear magnetic resonance (^{1}H-NMR) spectrum demonstrated the successful synthesis of the HA-PG conjugate (Figure S1, Supporting Information). The synthesized HA-PG conjugates exhibited self-crosslinking abilities due to the unique autoxidative properties of the PG groups, and this was inspired by the rapid self-regeneration of marine ascidians.[22] The HA-PG patches were easily fabricated by pouring the HA-PG solution into a pre-designed mold, which was followed by lyophilization.[23] When the lyophilized HA-PG patches absorbed liquids such as body fluid, the HA-PG conjugates in the hydrated patches began to self-crosslink via auto-oxidative coupling of PG groups even without any additives, ultimately forming crosslinked HA-PG hydrogel patches (Figure 2b). Notably, *in vivo* oxidative environments, such as those in which endogenous peroxidase and oxygen species are present, can facilitate the auto-oxidation of PG groups and consequently promote oxidative crosslinking of the HA-PG hydrogel patches.[25]

Thus, HA-PG hydrogel patches were prepared using horseradish peroxidase (HRP) to induce *in vivo*-like crosslinking. The storage moduli (G') of HA-PG hydrogels crosslinked with phosphate buffer saline (PBS) and HRP solutions were consistently higher than their respective loss moduli (G'') throughout the measured frequency ranges, thus indicating that the crosslinked HA-PG hydrogel patches behaved as stable and viscoelastic solids (Figure 2c). The average elastic modulus of the HA-PG hydrogels prepared via *in vivo*-like crosslinking using HRP was significantly higher than that of the HA-PG hydrogels crosslinked via spontaneous oxidation with PBS (Figure 2d). This was attributed to the enhanced oxidation of PG groups by the peroxidase enzyme to simulate oxidative environments *in vivo*. Thus, the HA-PG hydrogel patches crosslinked *in vivo* are likely to show stable and prolonged retention in the tissues. Furthermore, in the amplitude sweep mode, the G' values of both HA-PG hydrogels prepared with PBS and HRP were higher than their G'' values up to 100% of the applied strain (Figure S2, Supporting Information), indicating that the HA-PG patches possess sufficient mechanical properties to be applied to expandable and stretchable tissues such as skin tissue.

In addition to the self-crosslinking ability, the PG groups and their oxidative intermediates can noncovalently and covalently interact with various functional groups on the tissues, which contributes to the tissue-adhesiveness of HA-PG hydrogel patches.[22, 26] The tissue-adhesiveness of HA-PG patches on porcine skin tissues was measured in a tack test mode to obtain the force-displacement graphs (Figure 2e). Although the HA-PG hydrogel patch crosslinked via spontaneous oxidation with PBS (PBS group) exhibited tissue-adhesive properties the adhesive force of the HA-PG patch crosslinked via *in vivo*-like oxidation using HRP (HRP group) was ~4.11-fold greater than that of the HA-PG patch crosslinked using PBS (Figure 2f). We speculate that *in vivo*-like oxidation using HRP produces more oxidative intermediates of PG compared with spontaneous oxidation, thereby increasing covalent bonding with various nucleophilic moieties on the surface of tissues. This in turn

enhances tissue adhesion of the HA-PG patch. Likewise, the adhesion energy in the HRP-crosslinked patch group was ~ 3.73-fold higher than that in the PBS-crosslinked patch group (Figure 2g), and this was attributed to the enhanced mechanical properties and interfacial adhesiveness due to the *in vivo*-like oxidation using HRP. Taken together, our data indicated that the HA-PG patch was expected to show prominent self-crosslinking abilities and excellent tissue-adhesiveness in the oxidative environments *in vivo*.

2.2. The HA-PG patches with PTD-DBM and/or VPA promoted wound healing and suppressed scar formation in mice

The adhesive HA-PG hydrogel patch exhibits great potential as a sustained drug delivery system due to the high affinity of PG and its oxidized intermediates for various functional groups in biomolecules such as proteins, peptides, and chemicals. Thus, in this study, the HA-PG patches were tested as drug-loaded hydrogel dressings to facilitate the efficient delivery of therapeutic drugs into skin tissues to promote wound healing. As a drug delivery system, the release behavior of PTD-DBM and VPA was first investigated in the drug-loaded HA-PG patch. The HA-PG hydrogel patch was mainly made of HA, one of the abundant components of ECM. Thus, the HA-PG hydrogel patch can be degraded after application onto the wound by various molecules, especially the enzyme hyaluronidase, through regeneration processes. To evaluate the release profiles of encapsulated PTD-DBM and VPA, we collected and quantified the drugs released from the drug-loaded HA-PG patches with and without hyaluronidase at pre-determined timepoints (Day 1, 3, 7, and 10), considering the period of murine wound healing. In the PTD-DBM release profiles of patches loaded only with PTD-DBM, the PTD-DBM was sustainedly released over 10 d without an initial burst release

in both PBS and hyaluronidase-treated conditions (Figure S3a, Supporting Information). As expected, the drug release was slightly faster in the hyaluronidase-treated condition than in the PBS condition, but the sustained release was sufficiently achieved for 10 d. By contrast, in the VPA release profile for patches loaded only with VPA, approximately 90% of VPA was released on day 1, and most of the remaining VPA was released on day 3 (Figure S3b, Supporting Information). Presumably, efficient release of VPA, a GSKβ inhibitor that triggers the initial activation of the Wnt/β-catenin pathway, along with sustained release of PTD-DBM, which inhibits the function of CXXC5, a negative feedback regulator of this pathway, can further activate the Wnt/β-catenin pathway. The synergistic release profiles of both substances would be achieved due to the definite differences in molecular weight and binding affinity with phenolic PG groups between the relatively larger peptide (PTD-DBM) with various functional groups and the small molecular compound (VPA) with a simple structure.[27, 28] Notably, the drug release behaviors in the release profiles of PTD-DBM or VPA of the PTD-DBM+VPA-loaded patch were quite similar to those of the single drug-loaded patches, indicating that the HA-PG patch is an adequate system for dual delivery of synergistic drugs without interfering with the release behavior of either drug (Figure S2c, d, Supporting Information).

Before the skin regeneration test, the biocompatibility of the HA-PG patch was investigated. The cytotoxicity of the HA-PG was evaluated by culturing mouse embryonic fibroblasts in a hydrogel-conditioned medium, which was prepared by incubating the HA-PG hydrogel patch in a culture medium. In the live/dead assay conducted 1 d after culture, the HA-PG hydrogel did not affect the viability of the fibroblast, regardless of its concentration (Figure S4a, Supporting Information). Furthermore, in the 3-(4,5-dimethylthiazol-2-yl)-2,5-diphenyltetrazolium bromide (MTT) assay, there was no statistically significant difference between the mitochondrial activity of cells treated with the

conditioned medium and that of cells treated with the control medium (Figure S4b, Supporting Information). These results demonstrate that the HA-PG hydrogel patch did not induce cytotoxicity.

Skin regeneration by the HA-PG patch was evaluated in 1 cm^2 full-thickness mouse wounds (Figure S5, Supporting Information). Topical treatment with PTD-DBM and/or VPA promoted cutaneous wound healing, and this effect was better than that of epidermal growth factor (EGF), a commercially available wound-healing agent (**Figure 3**a and Figure S6, Supporting Information). A single application of the HA-PG patches in combination with PTD-DBM and/or VPA to the wound site promoted cutaneous wound healing more efficiently than daily topical treatment with PTD-DBM and/or VPA (Figure 3a and Figure S6, Supporting Information). In addition, scar formation was reduced in the patch application group compared with the topical treatment group, and especially, scar formation was remarkably reduced in the HA-PG+PTD-DBM+VPA application group (Figure 3a). The HA-PG patch itself did not significantly affect wound healing compared with the control group (Figure 3a), suggesting that the skin delivery of the PTD-DBM and/or VPA was facilitated by the HA-PG patches, thereby promoting wound healing and attenuating scar formation. Histological analyses also showed that the PTD-DBM and/or VPA promoted wound healing, and scar formation was significantly inhibited in the patch application group compared with the topical treatment group, consistent with visual observation (Figure 3b). Any histopathological problems were not found in the patch-treated skin tissues, and the survival of the mice was completely unaffected by the patch application.

Quantitative analysis of scar size also showed that the application with HA-PG+PTD-DBM+VPA significantly suppressed scar formation during cutaneous wound healing (Figure 3c, d). Collectively, these data show that the HA-PG patches with PTD-DBM and/or VPA not only promote cutaneous wound healing but also inhibit scar formation.

2.3. The HA-PG patches with PTD-DBM and/or VPA induced regenerative healing and caused the wound to more closely resemble normal skin structure

Sustained myofibroblast differentiation and hyperproliferation in the wound dermis can lead to excessive scarring.[29, 30] To determine the effect of HA-PG patches on cell proliferation and myofibroblast differentiation in the wound dermis, the levels of proliferating cell nuclear antigen (PCNA), a marker for proliferation, and α-smooth muscle actin (α-SMA), a marker for myofibroblast differentiation, were measured in the wounds of both the topical treatment and patch application groups. The level of PCNA was significantly increased in both the epidermis and dermis when the PTD-DBM and/or VPA were topically applied to wounds, representing that the PTD-DBM and/or VPA promoted the formation of new granulation tissue during the proliferative phase of wound healing (**Figure 4**a, b). On the contrary, in the patch application group containing PTD-DBM and/or VPA, dermal proliferation was highly reduced (Figure 4a, b) while epidermal proliferation was maintained (Insets in Figure 4a), showing that the HA-PG patches loaded with PTD-DBM and/or VPA promoted entry into the remodeling phase of wound healing. Similarly, topical treatment with PTD-DBM and/or VPA significantly induced α-SMA-positive myoblasts (Figure 4a, c), whereas application of HA-PG patches with PTD-DBM and/or VPA significantly reduced the numbers of α-SMA-positive cells except for vascular smooth muscle cells (Insets in Figure 4a), which was observed in normal skin (Figure 4a, c). These observations demonstrate that HA-PG patches with PTD-DBM and/or VPA promoted regenerative healing, creating new skins that were similar to normal skin in structure.

A previous report demonstrated that *Col3*-deficient mice reveal increased myofibroblast differentiation and scar deposition, suggesting a role of Collagen III in scar attenuation.[31] To

determine the type of collagen induced in the patch-treated group, the levels of Collagen I and Collagen III, the major collagens involved in wound healing, were monitored in the wounds (Figure 4d). Topical treatment with PTD-DBM and/or VPA effectively increased the level of Collagen I, whereas the level of Collagen I, a fibrotic collagen, was not obviously changed in the patch-application group (Figure 4e). Intriguingly, Collagen III involved in regenerative wound healing was significantly induced by HA-PG patches with PTD-DBM and/or VPA (Figure 4e, f). Notably, the Collagen III/Collagen I ratio was significantly increased in the patch application group including PTD-DBM and/or VPA, but not in the topical treatment group, as shown in scarless fetal wound healing (Figure 4e, g).

To further elucidate the mechanisms underlying regenerative healing by HA-PG patches, we measured the levels of Wnt/β-catenin signaling and its target, Endothelin-1, which is known to be involved in the enhancement of regenerative capabilities, in the wounds.[32] Nuclear β-catenin was significantly increased in both the epidermis and dermis of wounds in response to the application of HA-PG patches loaded with PTD-DBM and/or VPA (Figure S7a and S8a, Supporting Information). Consistently, the HA-PG patches with PTD-DBM and/or VPA further increased the expression of Endothelin-1 in both the wound epidermis and dermis, indicating that the HA-PG patches with PTD-DBM and/or VPA further promoted skin regeneration through additional activation of this pathway (Figure S7b and S8b, Supporting Information).

2.4. The HA-PG patches with PTD-DBM and/or VPA activated stem cells, promoted angiogenesis, and reduced ROS in the wounds

Stem cells primarily contribute to scar-free fetal wound healing, whereas differentiated cells such as myofibroblasts are primarily involved in scarring in adult wound healing.[3] Based on this notion, we sought to investigate the regulation of stem cell populations in the wounds by HA-PG patches. CD105 is a marker for MSCs involved in the regulation of collagen synthesis, which may affect scar formation.[33] CD105 was barely detected in untreated adult wounds (**Figure 5**a, b), but the HA-PG patches loaded with PTD-DBM and/or VPA significantly increased the expression of CD105 in the wound dermis (Figure 5a and Figure S10a, Supporting Information). CD34 and Nestin, other types of stem cell markers, were also significantly induced in the wound dermis by application of the HA-PG patches with PTD-DBM and/or VPA, suggesting that different types of stem cells induced by HA-PG patches could coordinately modulate regenerative wound healing (Figure S9 and S10b, c, Supporting Information).

The MSCs present in the wound sites are involved in promoting angiogenesis and reducing ROS.[34] The expression of CD31, a marker of endothelial cells, was increased in the patch application group, especially in the group treated with HA-PG patches with PTD-DBM and VPA (Figure 5c, d). Moreover, the application of HA-PG patches with PTD-DBM and/or VPA significantly reduced the amount of ROS present in the wounds compared with control and topical treatment groups, as demonstrated by Dihydroethidium (DHE) staining (Figure 5e, f). The Wnt/β-catenin pathway is known to induce the expression levels of nuclear factor (erythroid-derived 2)-like 2 (Nrf2), a master regulator of antioxidant metabolism.[35] The patches with PTD-DBM and/or VPA induced the expression level of Nrf2, thus possibly suppressing the production of ROS (Figure S11, Supporting Information).

2.5. The HA-PG patches with PTD-DBM and/or VPA modulated chemokines and cytokines that may affect the attenuation of scar formation

Cytokines and chemokines may be potential therapeutic targets for reducing skin scarring.[36] C-X-C chemokine receptor type-3 (CXCR3) plays an important role in the attenuation of scar formation, and CXCR4 is involved in skin regeneration as a target of the Wnt/β-catenin pathway.[16, 37] Similar to the pattern reported in humans,[38] the expression of CXCR3 was critically increased in the wound epidermis by the HA-PG patches with PTD-DBM and/or VPA (**Figure 6**a, c). Moreover, the expression of CXCR4, which plays a pivotal role in tissue regeneration,[39] was widely induced in the wounds by application of the HA-PG patches with PTD-DBM and/or VPA (Figure 6a and Figure S12a, Supporting Information).

Depletion of macrophages or inflammatory cytokines reduces scar formation.[40, 41] The HA-PG patches with PTD-DBM and/or VPA dramatically reduced the number of cells positive for F4/80, a major macrophage marker, in the wounds (Figure 6b, d). Consistent with this finding, IL-6 expression was significantly reduced by the HA-PG patches loaded with PTD-DBM and/or VPA in both the wound epidermis and dermis (Figure 6b and Figure S12b, Supporting Information). Overall, these data indicate that the HA-PG patches together with PTD-DBM and/or VPA induced scar attenuation and skin regeneration through the dynamic regulation of chemokines and cytokines.

2.6. *Cxxc5*-deficient mouse fibroblasts recapitulated the regenerative healing phenotype induced by the HA-PG patches with PTD-DBM and/or VPA

To further elucidate the underlying mechanism of regenerative healing induced by the HA-PG patches, *Cxxc5*$^{+/+}$ and *Cxxc5*$^{-/-}$ mouse dermal fibroblasts were obtained by explant culture (**Figure 7**a). *Cxxc5*$^{-/-}$ mouse fibroblasts showed increased motility compared with *Cxxc5*$^{+/+}$ mouse fibroblasts after scratching of the cell monolayer, and VPA treatment further induced the cell migration in these *Cxxc5*$^{-/-}$ mouse fibroblasts (Figure 7b, c). Cxxc5 expression was completely abolished (Figure 7d, e), and β-catenin, particularly its nuclear expression, was induced in *Cxxc5*$^{-/-}$ mouse fibroblasts as indicated by immunocytochemical analysis (Figure 7d, f). The Cxxc5 deletion and/or VPA treatment critically induced Collagen III and the actin cytoskeleton, which are important for regenerative fetal healing,[3, 42] in the mouse dermal fibroblasts (Figure 7g-i).

To investigate the effect of HA on the expression of β-catenin or Cxxc5, we also treated the *Cxxc5*$^{+/+}$ and *Cxxc5*$^{-/-}$ mouse dermal fibroblasts with HA in the presence or absence of VPA. The HA slightly induced cell migration in the mouse dermal fibroblasts as reported in the previous literature,[43] but did not exert significant additive effects on cell migration with Cxxc5 deletion and/or VPA treatment (Figure 7b, c). Importantly, the HA itself had no effect on β-catenin or Cxxc5 expression, as indicated by immunocytochemical analyses (Figure 7d-f). In addition, the HA did not show any additive effect on Collagen III expression or cortical actin network along with Cxxc5 loss and/or VPA treatment (Figure 7g-i). These combined data indirectly suggest that the significant regenerative effect of the HA-PG patches with PTD-DBM and/or VPA is due to the improved penetration of materials by the patches rather than the HA itself.

3. Discussion

One of the major barriers to wound healing in adults is that scars remain in the healed tissues unlike the healing in fetuses.[3] The development of therapeutic agents to prevent scar formation is expected based on the observation that early gestation fetal skin wounds can repair without scarring.[5] Treatment of HA-PG patches loaded with VPA and a peptide interfering with the CXXC5-Dvl interaction resulted in a healing pattern that was similar to scarless fetal wound healing for several reasons. First, the high level of HA facilitates cellular movement and traps water during fetal wound healing or healing with HA-PG patches.[5] Second, the prominent accumulation of type III collagen, which cannot be induced by EGF application, plays a crucial role in cellular migration and regeneration during fetal wound healing, and HA-PG loaded with PTD-DBM and/or VPA significantly elevated the Collagen III/Collagen I in wounds.[2, 3] Third, the combination of HA-PG and a peptide inhibiting the CXXC5-Dvl interaction significantly reduced inflammatory cytokines as in fetal wounds.[3, 5] Fourth, CXCR3, which binds to anti-inflammatory chemokines such as CXCL9, CXCL10 and CXCL11, plays an important role in the process of epidermal and dermal maturation in fetal wound healing and healing using HA-PG loaded with both PTD-DBM and VPA.[37, 44] Fifth, MSCs such as CD105 and Nestin, which are involved in the attenuation of scar formation, are highly expressed in adult mice wounds treated with HA-PG+PTD-DBM+VPA or fetal wounds.[4, 34] Finally, *Cxxc5*$^{-/-}$ mouse fibroblasts recapitulated the phenotypes seen in adult wounds using HA-PG+PTD-DBM+VPA and in fetal wounds. Collectively, the combination of a peptide inhibiting the CXXC5-Dvl interaction and a Wnt/β-catenin signaling activator with an HA patch could provide a potential treatment for minimizing scarring by regulating various factors related to regenerative healing.

The Wnt/β-catenin pathway is essential for wound healing, but its effect on scar formation depends on the wound type.[45, 46] The Wnt/β-catenin pathway is dysregulated in fibroproliferative wounds such as keloids with excessive ECM accumulation, but activation of this pathway is certainly

needed for optimal wound healing in acute wounds with low ECM expression.[45, 46] The collagen deposition mediated by the Wnt/β-catenin pathway is indispensable for skin wound healing but has the potential to cause scarring.[47] Consistent with this notion, our results revealed that topical treatment with a peptide and/or agent activating the Wnt/β-catenin pathway significantly promoted wound healing, while the effect on scar formation was insignificant compared with the patch application group. However, notably, treatment of HA-PG patches loaded with PTD-DBM and/or VPA simultaneously promoted wound healing and scar maturation along with the induction of specific collagen such as Collagen III. Although a means to promote both wound healing and scarring mitigation from the standpoint of collagen regulation has long presented a conundrum to researchers, our findings can provide a striking and novel means to address this problem.

Previous reports have demonstrated that improper wound healing can lead to chronic wounds or cancer.[48] The close relationship between wound healing and cancer has long been well-known.[49] The mechanisms that control wound healing promote the transformation and growth of malignant cells by enhancing cancer stem cell (CSC) populations.[49] For instance, mice possessing a mutation in the phosphorylation site of GSK3β, which is associated with wound healing,[47] in the β-catenin gene exhibit a cancer phenotype.[50] However, the CXXC5-Dvl interaction is a safe therapeutic target that can be used to promote wound healing without cancer-like side effects for the following reasons.[12] *Cxxc5*$^{-/-}$ mice showed an accelerated wound healing phenotype, but no abnormalities including cancer were observed during the long-term breeding of these mice.[12] Moreover, PTD-DBM treatment does not increase c-Myc and Cyclin D1, which are related to cell transformation among the Wnt/β-catenin signaling targets, but only increases Endothelin-1 related to wound healing, and long-term treatment with PTD-DBM in the skin did not show any abnormalities

including cancer.[12] Overall, interfering with the CXXC5-Dvl interaction can promote regenerative wound healing without any side effects, including prominent scar formation.

4. Conclusion

In summary, in this study, we revealed that the HA-PG patches with PTD-DBM and/or VPA induced both cutaneous wound healing and scar mitigation by examining various markers related to wound healing and scar attenuation. Given the current situation where wound healing agents and scar emollients are being developed separately, our novel pro-regenerative material could be utilized as a potential therapeutic agent to promote both wound healing and scar mitigation. Furthermore, our off-the-shelf formulation of drug-combined bio-adhesive hydrogel patches could greatly improve the practical convenience and clinical outcomes of wound therapies.

5. Experimental Section

Synthesis of HA-PG conjugate: The HA-PG conjugate was synthesized via carbodiimide chemistry according to previously reported procedures.[22] Briefly, HA (molecular weight 200 kDa, Lifecore Biomedical, Chaska, USA) was fully dissolved in triple distilled water (TDW) at a concentration of 10 mg/ml. Then, 1-(3-Dimethylaminopropyl)-3-ethylcarbodiimide hydrochloride (EDC, Thermo Fisher Scientific, Waltham, USA) was added to the HA solution at a 1:1.5 molar ratio of HA and EDC and stirred for 15 min. N-hydroxysuccinimide (NHS, Sigma-Aldrich, St. Louis, USA) was then added to the solution at a 1:1 molar ratio of HA and NHS, and the solution was further stirred for 15 min at pH 5.5–6.0. After the activation of the carboxyl groups in HA, 5-hydroxydopamine hydrochloride (Sigma-

Aldrich) was added to the reaction solution at a 1:1 molar ratio of HA and 5-hydroxydopamine and stirred for 24 h with a consistent pH of 4.5–5.0. Unreacted chemicals and byproducts were removed by dialysis using a membrane with a cut-off of 6–8 kDa (Membrane Filtration Products Inc., Seguin, USA) against acidic PBS (Biosesang, Gyeonggi-do, Korea) and TDW. The resultant HA-PG conjugate was lyophilized and stored at 4ºC until further use. Synthesis of the HA-PG conjugate was confirmed by ^{1}H-NMR spectroscopy at 300 MHz (Bruker, Billerica, USA).

Preparation of HA-PG patches: The HA-PG patches were prepared according to previously reported procedures. [23] The synthesized HA-PG was dissolved in PBS at a concentration of 1% (w/v). The solution was then poured into pre-designed rectangular molds (1 cm × 1 cm) and completely lyophilized. The resultant HA-PG patch was stored at -20ºC before use to avoid moisture. Drug-loaded HA-PG patches were prepared as described above. The drug was dissolved into the HA-PG solution at a predetermined concentration, and the drug-loaded HA-PG solution was then poured into the mold and lyophilized.

Crosslinking of HA-PG patches: To induce crosslinking of the HA-PG patches to form hydrogels, neutral PBS or 6 U/ml of HRP (Sigma-Aldrich) solution was applied to the lyophilized HA-PG patches for self-crosslinking via *in vitro* spontaneous oxidation and *in vivo*-like oxidation, respectively, using a peroxidase enzyme.

Rheological analysis: All rheological analyses were conducted using a rheometer (MCR 102, Anton Paar, Ashland, Ashland, USA). The G′ and G′′ values of the crosslinked HA-PG patches were measured in a frequency sweep mode at the frequency range of 0.1–10 Hz, and the elastic moduli of the patches were determined by calculating the average storage modulus measured at 1 Hz. The moduli were also measured in amplitude sweep mode at an oscillatory strain range of 0.1–100% with a fixed frequency (1 Hz).

Evaluation of tissue-adhesiveness: To evaluate the tissue-adhesiveness of HA-PG patches, the interfacial adhesive forces of the patches to the tissue surface were measured using the MCR 102 rheometer in a tack test mode. Sliced porcine skin tissues were attached to the probe and stage in the rheometer, and the HA-PG patches were placed between them during oxidative crosslinking for 45 min. Then, the force required for detaching the hydrogel from the tissue surfaces was measured while pulling the probe at 10 μm/s. PBS was applied to the gap between the tissue surfaces as a control. The maximum adhesive force was determined by picking out the peak force in the measured force-displacement graph, and the adhesive energy was determined by calculating the area under the curve in the graph.

Evaluation of drug release behavior: To evaluate the release profiles of PTD-DBM and VPA from the HA-PG patches, PTD-DBM only-loaded HA-PG patches, VPA only-loaded HA-PG patches, and PTD-DBM+VPA-loaded HA-PG patches were prepared and crosslinked with 6 U/ml of HRP solution in PBS. PTD-DBM was fluorescently labelled by fluorescein isothiocyanate (FITC) for quantification. The crosslinked HA-PG patches were incubated in PBS and 50 U/ml hyaluronidase solution in PBS at 37°C,

respectively, and the supernatants were collected at predetermined timepoints (Day 1, 3, 7, and 10). The PTD-DBM in the supernatant was quatified by measuring a fluorescent signal using a microplate reader (Tecan, Männedorf, Switzerland), and the VPA in the supernatant was quantified by liquid chromatography mass spectrometry using a Q-exactive orbitrap plus (Thermo Fisher Scientific).

In vitro biocompatibility test: To evaluate *in vitro* biocompatibility, live/dead and MTT assays were conducted using an HA-PG hydrogel patch-conditioned medium. The conditioned medium was prepared by incubating the HA-PG hydrogel patches at two different concentration (1.0 and 2.0 mg/ml) in Dulbecco's Modified Eagle Medium (DMEM, Gibco, Gaithersburg, USA) supplemented with 10% fetal bovine serum (FBS, Gibco) and 1% penicillin/streptomycin (Gibco) at 37°C for 24 h. DMEM without the hydrogel conditioning served as a control. NIH 3T3 cells, a mouse embryonic fibroblast cell line, were seeded in a cell culture plate at a density of 9000 cells/cm^2. Then, the cells were treated with the conditioned medium and further cultured at 37°C for 24 h. The viability of the cells was visualized using a live/dead viability/cytotoxicity kit, according to the manufacturer's protocol and observed using a fluorescence microscope (IX73, Olympus, Tokyo, Japan). Cellular viability was also quantitatively evaluated by measuring the mitochondrial activity of the cells using a MTT (Sigma-Aldrich) assay, compared with the control group.

Mice and in vivo experimentation: All animal studies were approved by the Institutional Review Board of Severance Hospital, Yonsei University College of Medicine (IACUC-202201-1403-01). Mice were housed in separate ventilated mouse cages controlled by computerized control systems (Threeshine Inc., Seoul, Korea). All animal experiments complied with the ARRIVE guidelines.

Six-week-old male C3H mice obtained from Koatech Co. (Gyeonggi-do, Korea) were acclimatized to the new environment for 1 week and then used to determine the effect of HA-PG patches with PTD-DBM and/or VPA on wound healing and scar formation (*n* = 10 per group). Seven-week-old mice, whose hair follicles were in the telogen phase, were anesthetized with 2,2,2-tribromoethanol (Sigma Aldrich), and the hairs on their backs were shaved with a hair clipper. Full-thickness 1 cm^2 wounds were then created on the backs of mice and treated daily with vehicle (PBS) alone, 100 μM PTD-DBM alone, 50 mM VPA alone (Acros, Geel, Belgium), PTD-DBM and VPA combination, or 100 μM EGF (PeproTech, Princeton, USA) alone as topical treatment groups. For patch application, the HA-PG patches containing the indicated substances were applied once to the wounds.

Hematoxylin and eosin (H&E) staining: Wound tissues were fixed in 4% (w/v) paraformaldehyde (PFA) in PBS overnight at 4°C and then dehydrated, paraffinized, embedded in paraffin, and sliced into a 4-μm thickness. Sections were deparaffinized and rehydrated by incubation in a series of xylene and graded ethanol. The slides were incubated with Harris hematoxylin for 5 min and eosin for 1 min. The H&E-stained slides were observed under a bright-field optical microscope (ECLIPSE TE2000-U, Nikon, Tokyo, Japan).

Immunohistochemistry: The 4-μm paraffin sections were deparaffinized and rehydrated. For antigen retrieval, the slides were autoclaved in 10 mM sodium citrate buffer. After cooling, the slides were pre-incubated in PBS and blocked with 5% bovine serum albumin (BSA) in PBS for 30 min at room temperature. The slides were incubated overnight at 4°C with the following dilutions of primary

antibodies: anti-Keratin 14 (1:1000, BioLegend, San Diego, USA), anti-PCNA (1:500, Santa Cruz Technology, Dallas, USA), anti-α-SMA (1:200, Abcam, Cambridge, USA), anti-Collagen I (1:200, Abcam), anti-Collagen III (1:200, Novus Biologicals, Littleton, USA), anti-CD105 (1:50, R&D Systems, Minneapolis, USA), anti-CD31 (1:100, Abcam), anti-β-catenin (1:100, BD Biosciences, Lexington, USA), anti-Endothelin-1 (Novus Biologicals, 1:50), anti-Nestin (1:50, BD Biosciences), or anti-CD34 (1:100, Abcam). After washing with PBS, the slides were incubated with Alexa Fluor 488- or Alexa Fluor 555-conjugated IgG secondary antibody (1:500, Invitrogen, Carlsbad, USA) at room temperature for 1 h, and then stained with 4',6-diamidino-2-phenylindole (DAPI, 1:5000, Boehringer Mannheim, Ingelheim am Rhein, Germany) for 10 min. The stained images were examined using a Nikon Eclipse Ti microscope (Nikon).

For 3,3-diaminobenzidine (DAB) staining, the antigen retrieval was performed in the same manner as that used for immunofluorescence. To block endogenous peroxidase activity, the sections were incubated with 1% H_2O_2 (Samchun Chemicals, Gyeonggi-do, Korea) for 10 min. The sections were then incubated with the following primary antibodies overnight at 4°C: anti-Nrf2 (1:50, Thermo Fisher Scientific), anti-CXCR3 (1:100, Novus Biologicals), anti-CXCR4 (1:100, Novus Biologicals), anti-F4/80 (1:50, Santa Cruz Technology), or anti-IL-6 (1:500, Novus Biologicals). The next day, the sections were incubated with biotinylated secondary antibodies (1:200, Dako, Hamburg, Germany) for 1 h at room temperature. Then, the samples were incubated with avidin-HRP solution (VECTASTAIN® ABC kit, Vector Laboratories, Burlingame, USA) for 30 min, stained with DAB (Dako), and counterstained with Mayer's hematoxylin (Muto, Tokyo, Japan). The signals were analyzed using a bright-field microscope (Nikon TE-2000U).

DHE staining: The 20-µm frozen sections were pre-incubated with PBS for 5 min. 10 µM DHE (v/v) in PBS was prepared using a stock solution of 10 mM DHE (w/v) in dimethyl sulfoxide (DMSO). After incubating with 10 µM DHE staining solution in a dark chamber for 30 min at room temperature, the slides were counterstained with DAPI for 10 min.

Explant cell culture: *Cxxc5* heterozygous mice were bred for four generations to obtain wild-type littermates and *Cxxc5*$^{-/-}$ mice. The surgical instruments were sterilized prior to experimentation, and the *Cxxc5*$^{+/+}$ and *Cxxc5*$^{-/-}$ mice were euthanized. The skin was peeled off with sterile forceps and transferred to a petri dish containing PBS on ice. After removing the connective tissues under the dermis, the mouse skins were split into smaller pieces. The *Cxxc5*$^{+/+}$ and *Cxxc5*$^{-/-}$ mice skin explants were placed with the dermis facing down in a 24-well plate containing DMEM with 15% (v/v) FBS (Gibco), 100 mg/ml penicillin (Gibco), and 100 mg/ml streptomycin (Gibco). A few weeks after plating the *Cxxc5*$^{+/+}$ and *Cxxc5*$^{-/-}$ mouse skin explants, the cells were observed migrating from the skin dermis, and they were then detached and transferred into a larger dish.

In vitro wound healing assay: The *Cxxc5*$^{+/+}$ and *Cxxc5*$^{-/-}$ mouse dermal fibroblasts were plated into 12-well plates in DMEM supplemented with 15% FBS and were allowed to attach overnight. The monolayers were then gently scratched with sterile pipette tips and incubated in a medium containing 5% FBS with 1 mg/ml HA and/or 100 µM VPA. At 24 h after scratching, the cells were rinsed once with cold PBS, fixed in 4% PFA for 15 min at room temperature, and stained with 2% (w/v) crystal violet.

Immunocytochemistry: The *Cxxc5*$^{+/+}$ and *Cxxc5*$^{-/-}$ mouse dermal fibroblasts were seeded into 12-well culture plates at a density of 8×10^4 cells/well. The cells were washed with PBS before being fixed with 4% (w/v) PFA in PBS for 15 min at room temperature. Then, the cells were rinsed with PBS and permeabilized using 0.1% (v/v) Triton X-100 in PBS for 15 min. After washing with PBS, the cells were incubated with 5% BSA in PBS for 30 min and then incubated at 4°C overnight with following primary antibodies: anti-Cxxc5 (1:50, Santa Cruz Biotechnology), anti-β-catenin (1:100, BD Biosciences), or anti-Collagen III (1:200, Novus Biologicals). The cells were washed in PBS, and this was followed by incubation with Alexa Fluor 488- or Alexa Fluor 555-conjugated IgG secondary antibody (1:500, Invitrogen) in a dark chamber at room temperature for 1 h. The nuclei were counterstained with DAPI for 10 min. Actin filaments were labeled with Alexa Fluor® 555 Phalloidin (1:20, Cell Signaling Technology, Danvers, USA) for 15 min. The stained images were acquired with the Nikon Eclipse Ti microscope (Nikon).

Quantification of immunostaining: Immunohistochemical and immunocytochemical staining was quantified using NIS Elements V3.2 software (Nikon). The thresholds were defined as red, green, and blue channels, where the blue channels were used to represent the nuclei. The mean intensity was measured separately for the red and green channels, and the mean value was estimated by measuring the results of at least three independent experiments.

Statistical analysis: Data are represented as the means ± Standard Deviation (SD). Statistical analyses were performed by using the Student's *t*-test or two-way ANOVA test in GraphPad Prism V6.01 (GraphPad Software, Inc., San Diego, CA). The sample size used for each analysis is clearly stated in each figure legend, and statistical significance is presented in the figures as follows: **P* <0.05, ***P* <0.01, and ****P* <0.001.

Supporting Information

Supporting Information is available from the Wiley Online Library or from the author.

Acknowledgements

S.-H. L. and S. A. contributed equally to this work. This work was supported by the National Research Foundation of Korea (NRF) grant funded by the Korean Government (MSIT) (2019R1A2C3002751, 2020M3E5E2040018). This work was also supported by the Korea Evaluation Institute of Industrial Technology (KEIT) grant funded by the Korea Government (MSIT) (20009125). S.-H. L. was supported by National Research Foundation of Korea (NRF) through Creative Challenge Research Foundation Support Project (2022R1I1A1A01073599).

Conflict of Interest

The authors declare that they have no known competing financial interests or personal relationships that could have appeared to influence the work reported in this paper.

Authors Contribution

S.-H. L.: Conception, Methodology, Experiment conduction, Analysis, and Writing. S. A.: Material preparation, Experiment conduction, and Writing. Y. C. R.: Experiment conduction. S. H. S.: Experiment conduction. S. P.: Experiment conduction. M. J. L.: Material preparation. S.-W. C.: Conception and Writing. K.-Y. C.: Supervision, Conception, and Writing.

Data Availability Statement

All data generated or analyzed during this study are included in this published article. The data that support the findings of this study are available from the corresponding author upon reasonable request.

Received: ((will be filled in by the editorial staff))
Revised: ((will be filled in by the editorial staff))
Published online: ((will be filled in by the editorial staff))

References

[1] C. M. Brewer, B. R. Nelson, P. Wakenight, S. J. Collins, D. M. Okamura, X. R. Dong, W. M. Mahoney Jr, A. McKenna, J. Shendure, A. Timms, *Dev. Cell* **2021**, 56, 2722.

[2] G. C. Gurtner, S. Werner, Y. Barrandon, M. T. Longaker, *Nature* **2008**, 453, 314.

[3] M. Monavarian, S. Kader, S. Moeinzadeh, E. Jabbari, *Tissue Eng. Part B Rev.* **2019**, 25, 294.

[4] A. L. Moore, C. D. Marshall, L. A. Barnes, M. P. Murphy, R. C. Ransom, M. T. Longaker, *Wiley Interdiscip. Rev. Dev. Biol.* **2018**, 7, e309.

[5] B. J. Larson, M. T. Longaker, H. P. Lorenz, *Plast. Reconstr. Surg.* **2010**, 126, 1172.

[6] J. O. Brant, J. H. Yoon, T. Polvadore, W. B. Barbazuk, M. Maden, *Wound Repair Regen.* **2016**, 24, 75.

[7] M. Ito, Z. Yang, T. Andl, C. Cui, N. Kim, S. E. Millar, G. Cotsarelis, *Nature* **2007**, 447, 316.

[8] S.-H. Lee, S. H. Seo, D.-H. Lee, L.-Q. Pi, W.-S. Lee, K.-Y. Choi, *J. Invest. Dermatol.* **2017**, 137, 2260.

[9] S.-H. Lee, J. Yoon, S. H. Shin, M. Zahoor, H. J. Kim, P. J. Park, W.-S. Park, D. S. Min, H.-Y. Kim, K.-Y. Choi, *PLoS One* **2012**, 7, e34152.

[10] S.-H. Lee, M. Zahoor, J.-K. Hwang, D. S. Min, K.-Y. Choi, *PLoS One* **2012**, 7, e48791.

[11] D. Zhang, L. Gu, L. Liu, C. Wang, B. Sun, Z. Li, C. Sung, *Biochem. Biophys. Res. Commun.* **2009**, 378, 149.

[12] S.-H. Lee, M.-Y. Kim, H.-Y. Kim, Y.-M. Lee, H. Kim, K. A. Nam, M. R. Roh, D. S. Min, K. Y. Chung, K.-Y. Choi, *J. Exp. Med.* **2015**, 212, 1061.

[13] J. H. Yoon, K. Cho, T. J. Garrett, P. Finch, M. Maden, *Sci. Rep.* **2020**, 10, 1.

[14] D. Naor, *Front. Immunol.* **2016**, 7, 39.

[15] J. M. S. Garcia, A. Panitch, S. Calve, *Acta biomaterialia* **2019**, 84, 169.

[16] H. Chen, G. Li, Y. Liu, S. Ji, Y. Li, J. Xiang, L. Zhou, H. Gao, W. Zhang, X. Sun, *Front. Immunol.* **2021**, 12, 668758.

[17] A. Weich, D. Rogoll, S. Gawlas, L. Mayer, W. Weich, J. Pongracz, T. Kudlich, A. Meining, M. Scheurlen, *Diagnostics* **2021**, 11, 367.

[18] J. Liu, Q. Xiao, J. Xiao, C. Niu, Y. Li, X. Zhang, Z. Zhou, G. Shu, G. Yin, *Signal Transduct. Target. Ther.* **2022**, 7, 1.

[19] J. Whyte, A. Smith, J. Helms, *Cold Spring Harb. Perspect. Biol.* **2012**, 4, a008078.

[20] N. R Johnson, Y. Wang, *Curr. Pharm. Biotechnol.* **2015**, 16, 621.

[21] S. Choi, J. S. Lee, J. Shin, M. S. Lee, D. Kang, N. S. Hwang, H. Lee, H. S. Yang, S.-W. Cho, *J. Control. Release* **2020**, 327, 571.

[22] J. H. Cho, J. S. Lee, J. Shin, E. J. Jeon, S. An, Y. S. Choi, S. W. Cho, *Adv. Funct. Mater.* **2018**, 28, 1705244.

[23] J. Shin, S. Choi, J. H. Kim, J. H. Cho, Y. Jin, S. Kim, S. Min, S. K. Kim, D. Choi, S. W. Cho, *Adv. Funct. Mater.* **2019**, 29, 1903863.

[24] S. An, E. J. Jeon, S. Y. Han, J. Jeon, M. J. Lee, S. Kim, M. Shin, S. W. Cho, *Small* **2022**, 18, 2202729.

[25] J. S. Lee, J. H. Cho, S. An, J. Shin, S. Choi, E. J. Jeon, S.-W. Cho, *Chem. Mater.* **2019**, 31, 9614.

[26] Y. Hino, H. Ejima, *J. Photopolym. Sci. Technol.* **2020**, 33, 123.

[27] W. Zhang, R. Wang, Z. Sun, X. Zhu, Q. Zhao, T. Zhang, A. Cholewinski, F. K. Yang, B. Zhao, R. Pinnaratip, *Chem. Soc. Rev.* **2020**, 49, 433.

[28] H. Ding, B. Li, Y. Jiang, G. Liu, S. Pu, Y. Feng, D. Jia, Y. Zhou, *Carbohydr. Polym.* **2021**, 251, 117101.

[29] Y. Liu, Y. Li, N. Li, W. Teng, M. Wang, Y. Zhang, Z. Xiao, *Sci. Rep.* **2016**, 6, 1.

[30] M. A. Nishiguchi, C. A. Spencer, D. H. Leung, T. H. Leung, *Cell Rep.* **2018**, 24, 3383.

[31] S. W. Volk, Y. Wang, E. A. Mauldin, K. W. Liechty, S. L. Adams, *Cells Tissues Organs* **2011**, 194, 25.

[32] I. Hwang, E. J. Lee, H. Park, D. Moon, J. N. Park, K. C. Kim, A. Cha, H. Yun, J. Lee, H.-W. Park, *Biomaterials* **2021**, 275, 120980.

[33] A. Rodríguez-Barbero, J. Obreo, P. Álvarez-Muñoz, A. Pandiella, C. Bernabéu, J. M. López-Novoa, *Cell. Physiol. Biochem.* **2006**, 18, 135.

[34] W. M. Jackson, L. J. Nesti, R. S. Tuan, *Stem Cell. Res. Ther.* **2012**, 3, 1.

[35] P. Rada, A. I. Rojo, A. Offergeld, G. J. Feng, J. P. Velasco-Martín, J. M. González-Sancho, A. M. Valverde, T. Dale, J. Regadera, A. Cuadrado, *Antioxidants & redox signaling* **2015**, 22, 555.

[36] P. A. Rees, N. S. Greaves, M. Baguneid, A. Bayat, *Adv. Wound Care* **2015**, 4, 687.

[37] C. C. Yates, P. Krishna, D. Whaley, R. Bodnar, T. Turner, A. Wells, *Am. J. Pathol.* **2010**, 176, 1743.

[38] E. Bünemann, N.-P. Hoff, B. A. Buhren, U. Wiesner, S. Meller, E. Bölke, A. Müller-Homey, R. Kubitza, T. Ruzicka, A. Zlotnik, *Eur. J. Med. Res.* **2018**, 23, 1.

[39] M. E. Bianchi, R. Mezzapelle, *Front. Immunol.* **2020**, 11, 2109.

[40] Y. Feng, Z.-L. Sun, S.-Y. Liu, J.-J. Wu, B.-H. Zhao, G.-Z. Lv, Y. Du, S. Yu, M.-L. Yang, F.-L. Yuan, *Front. Physiol.* **2019**, 10, 1101.

[41] Z.-C. Wang, W.-Y. Zhao, Y. Cao, Y.-Q. Liu, Q. Sun, P. Shi, J.-Q. Cai, X. Z. Shen, W.-Q. Tan, *Front. Immunol.* **2020**, 11, 603187.

[42] X. L. Strudwick, A. J. Cowin, *Cells* **2012**, 1, 1313.

[43] D. Andreutti, A. Geinoz, G. Gabbiani, *J. Submicrosc. Cytol. Pathol.* **1999**, 31, 173.

[44] S. Balaji, C. L. Watson, R. Ranjan, A. King, P. L. Bollyky, S. G. Keswani, *Adv. Wound Care* **2015**, 4, 660.

[45] J. Bukowska, K. Walendzik, M. Kopcewicz, P. Cierniak, B. Gawronska-Kozak, *Connect. Tissue Res.* **2021**, 62, 238.

[46] M. Sato, *Acta Derm. Venereol.* **2006**, 86.

[47] M. Kapoor, S. Liu, X. Shi-Wen, K. Huh, M. McCann, C. P. Denton, J. R. Woodgett, D. J. Abraham, A. Leask, *J. Clin. Investig.* **2008**, 118, 3279.

[48] G. M. Sundaram, S. Quah, P. Sampath, *FEBS J.* **2018**, 285, 4516.

[49] K. M. Arnold, L. M. Opdenaker, D. Flynn, J. Sims-Mourtada, *Cancer Growth Metastasis* **2015**, 8, 1.

[50] E. R. Deschene, P. Myung, P. Rompolas, G. Zito, T. Y. Sun, M. M. Taketo, I. Saotome, V. Greco, *Science* **2014**, 343, 1353.

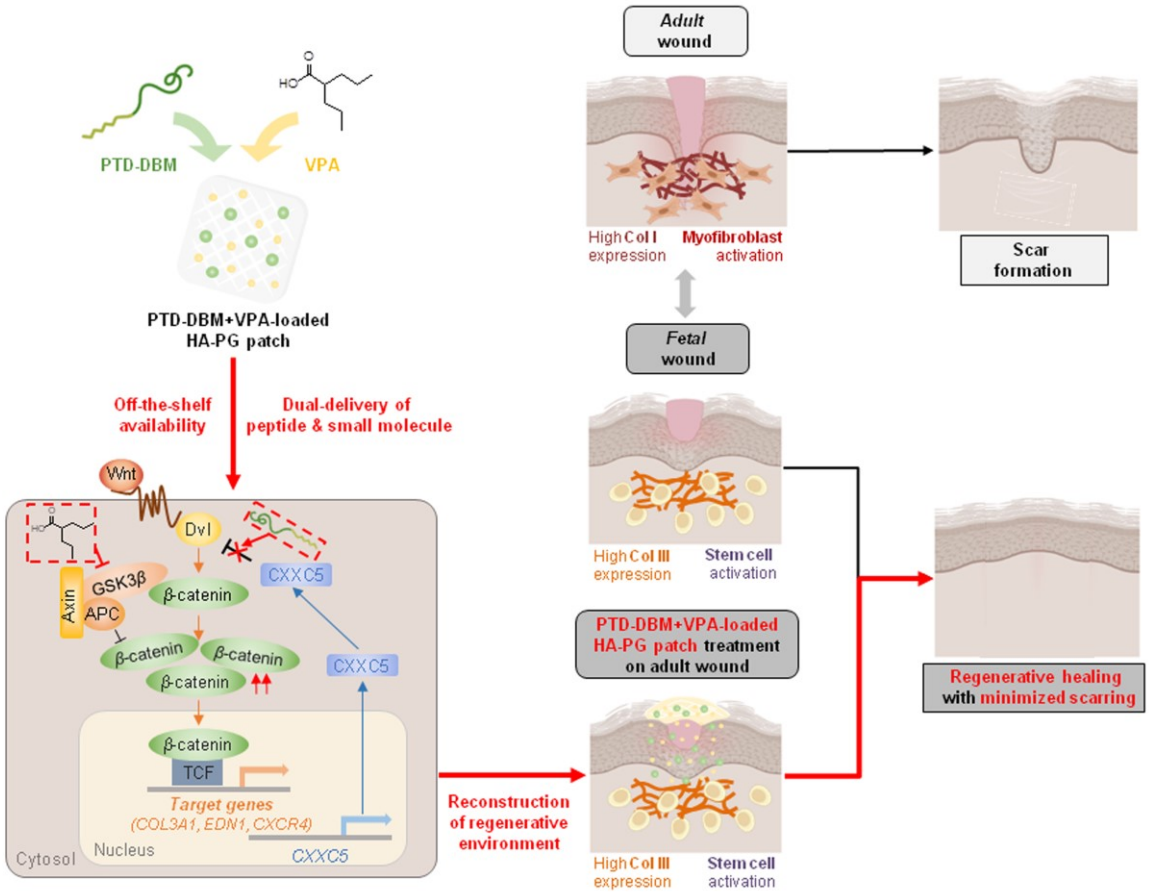

Figure 1. Schematic illustration showing the mechanism underlying regenerative healing induced by HA-GA patches loaded with PTD-DBM and VPA. The HA-PG patches allow for off-the-shelf availability and dual delivery of PTD-DBM and VPA, and reconstruct the regenerative microenvironment during wound healing, providing regenerative healing while minimizing scarring.

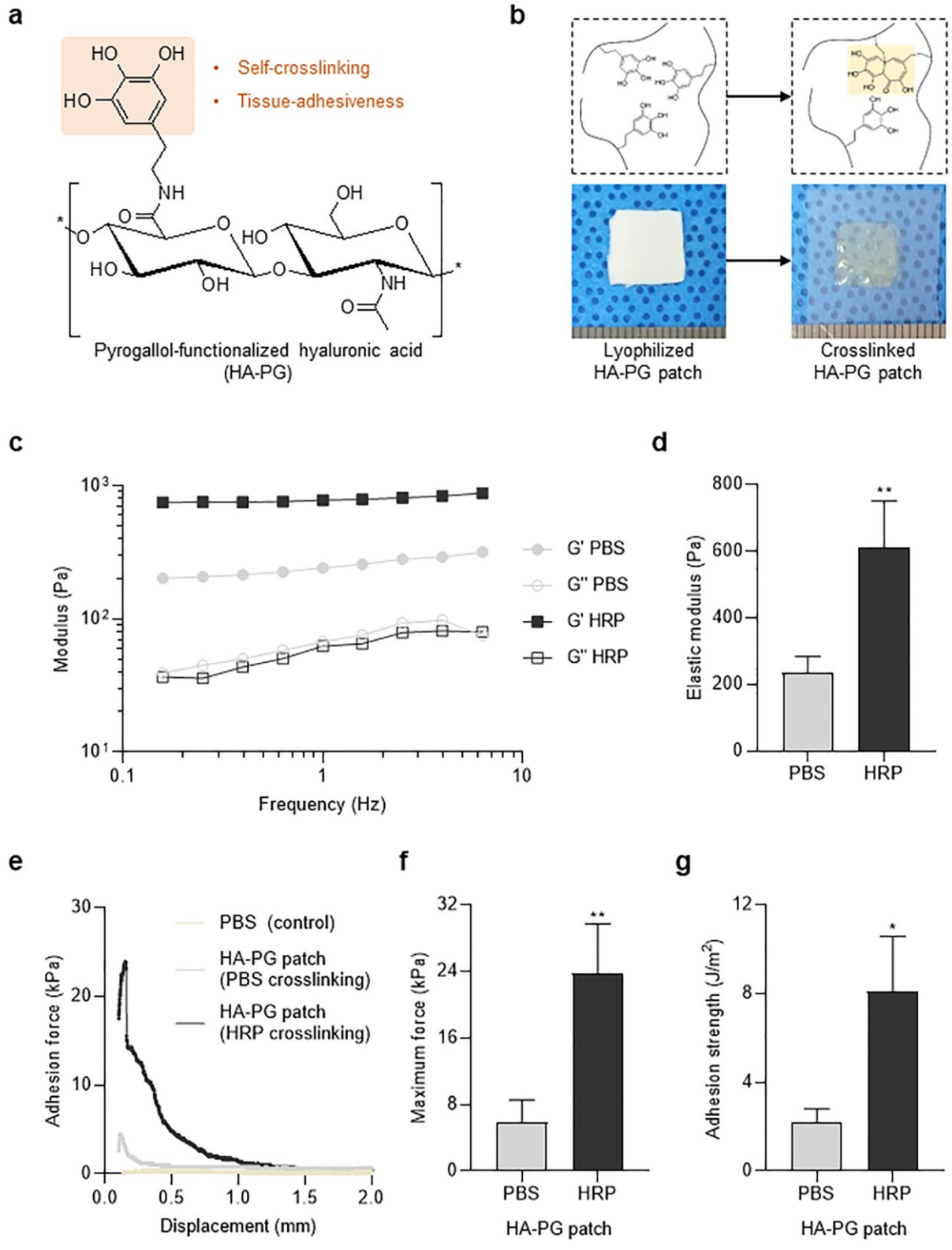

Figure 2. The HA-PG patches exhibited self-crosslinking and tissue-adhesiveness. a) Chemical structure of the HA-PG conjugate. b) Photographs and internal chemical structures of the lyophilized HA-PG patch and the HA-PG hydrogel patch after self-crosslinking via spontaneous oxidation with PBS. c) Storage modulus (G′) and loss modulus (G″) of HA-PG hydrogel patches crosslinked via spontaneous oxidation with PBS (PBS group) and *in vivo*-like oxidation with HRP solution (HRP group), respectively. d) Average elastic modulus of the HA-PG hydrogel patches in the PBS and HRP groups (n = 4). e) Representative force-displacement graph measuring the adhesion forces of PBS and HA-PG hydrogel patches on porcine skin tissues in the PBS and HRP groups. f) Average maximum forces and g) adhesion strengths of HA-PG patches in the PBS and HRP groups (n = 3). The Student's t-test was used for statistical analysis. Data are presented as means ± SD. *P <0.05, **P <0.01 for panels d), f), and g).

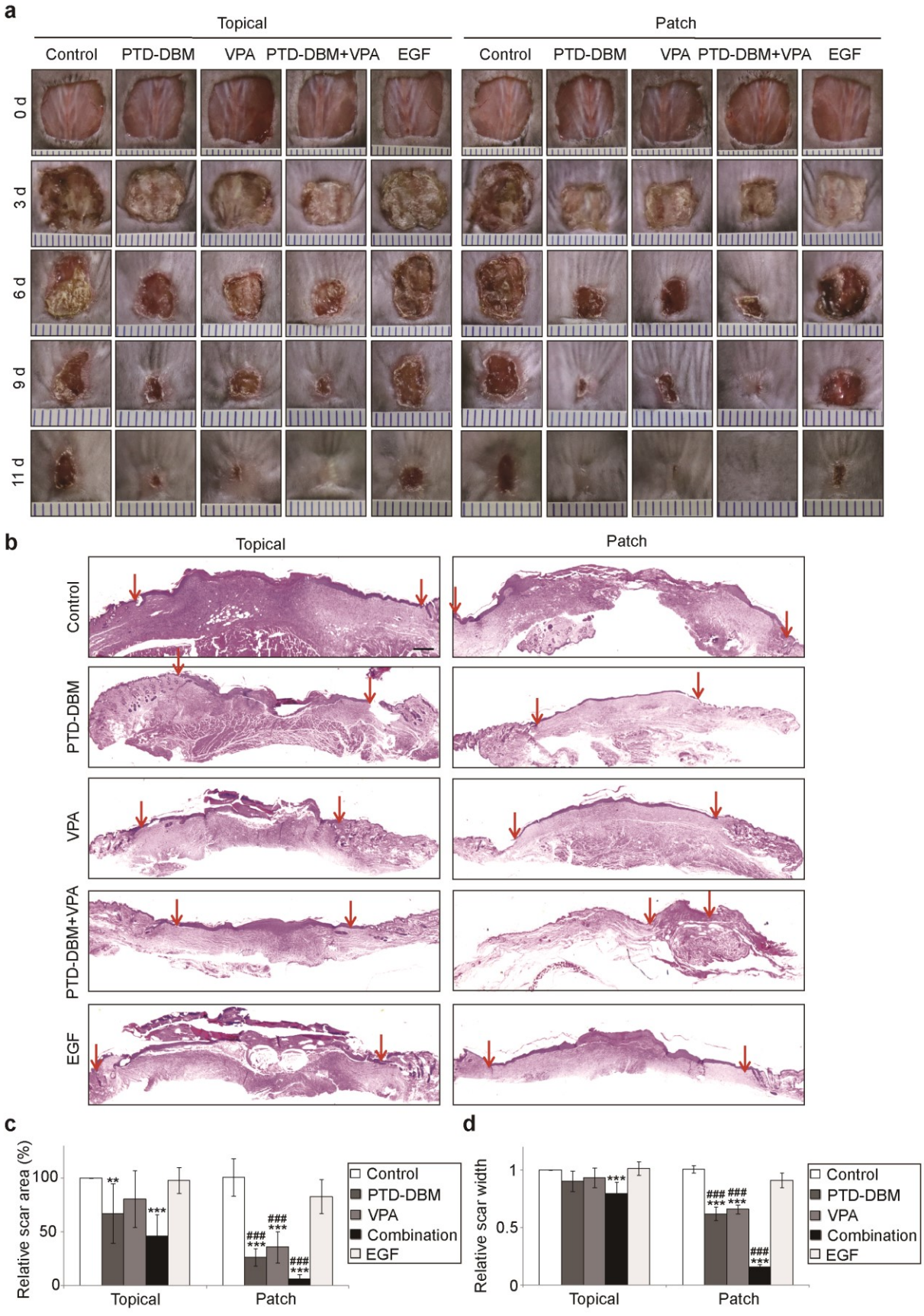

Figure 3. The HA-PG patches loaded with PTD-DBM and/or VPA accelerated wound healing and inhibited scar formation. a) Representative images of wounds on the backs of 7-week-old mice that received topical or HA-PG-mediated treatments with the indicated materials on days 0, 3, 6, 9, and 11 after wounding (*n* = 10 per group). b) H&E staining of the wound tissues of mice applied topically or via the HA-PG patches with the indicated materials 11 days post-wounding. Red arrows indicate the scar margins. Scale bar, 500 μm. c) Measurements of scar area on the 11th day post-wounding as assessed using the Image J program (*n* = 10). d) Measurements of scar width using H&E-stained sections from wound tissues on the 11th day post-wounding using the Image J program (*n* = 5). The two-way ANOVA test was used for statistical analysis. Data are represented as means ± SD. ***P* <0.01, ****P* <0.001 compared with the control group; ###*P* <0.001 compared with the topical treatment group for panels c) and d).

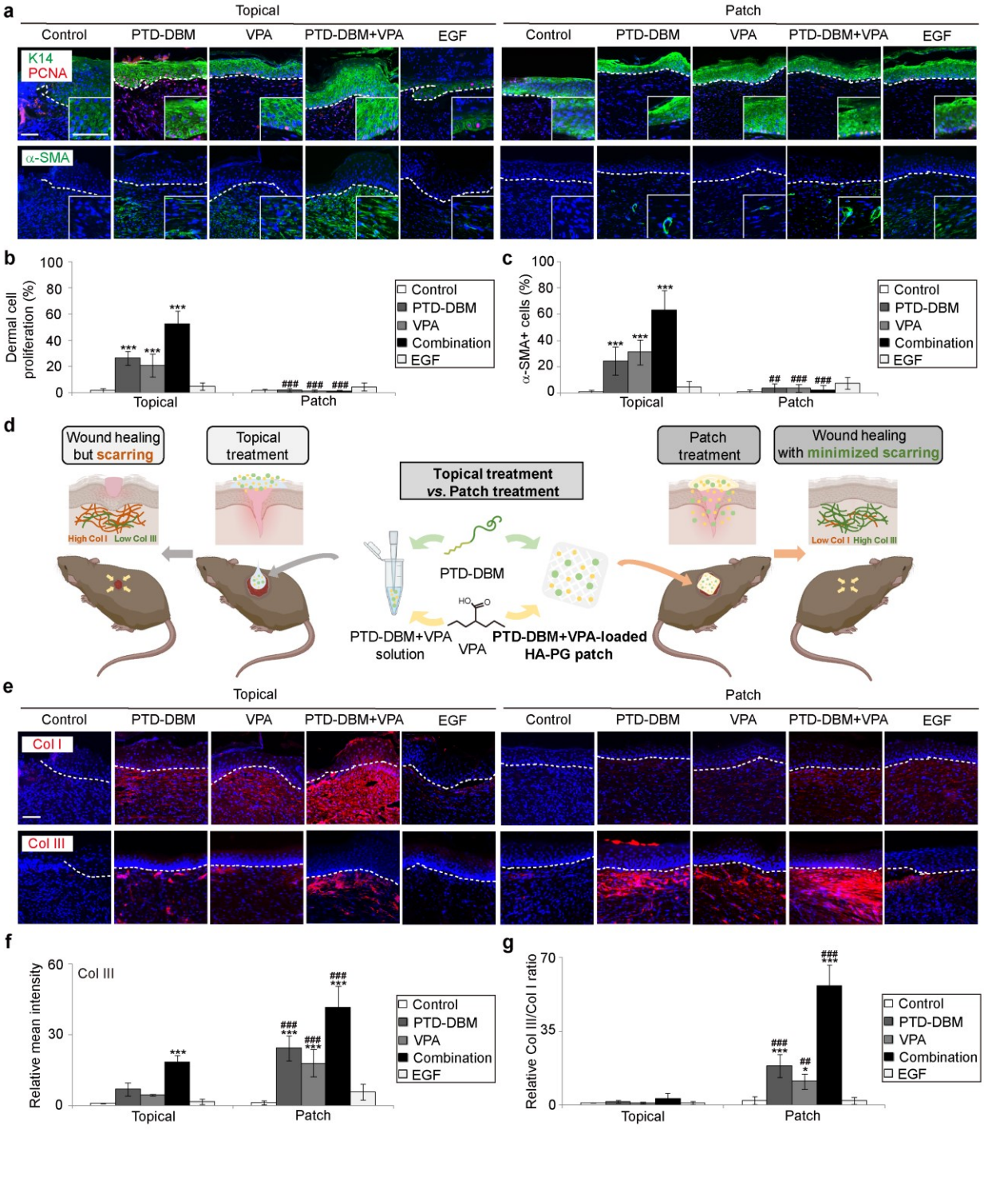

Figure 4. The HA-PG patches with PTD-DBM and/or VPA induced the regenerative wound healing.

a) Immunohistochemical staining for Keratin 14 (green, upper panel), PCNA (red, upper panel), and

α-SMA (green, lower panel) with DAPI nuclear counterstaining (blue) in the wounds that received topical or HA-PG-mediated treatments with the indicated substances on the 11th day post-wounding. The dashed lines represent the epidermis–dermis border in the wounds. The upper panel insets indicate that PCNA expression is maintained in the Keratin 14-positive epidermis, and the lower panel insets indicate that α-SMA is mainly expressed in vascular smooth muscle cells but not myofibroblasts after application of the HA-PG patches with PTD-DBM and/or VPA. Scale bar, 75 μm. b) Quantification of PCNA-positive cells in the wound dermis (*n* = 5). c) Quantification of α-SMA-positive cells in the wound dermis (*n* = 5). d) Schematic depicting the experimental design for determining the type of collagen induced by topical or patch-mediated treatment. e) Immunohistochemical staining for Collagen I (red, upper panel) and Collagen III (red, lower panel) with DAPI staining (blue) in the wounds applied topically or via patches with the indicated substances 11 days post-wounding. Scale bar, 75 μm. f) Mean intensity quantification of Collagen III in the wound dermis (*n* = 5). g) Quantification of the Collagen III/Collagen I ratio after measuring the mean intensity of each type of collagen (*n* = 5). The two-way ANOVA test was used to determine statistically significant differences. Data are presented as means ± SD. **P* <0.05, ****P* <0.001 versus the control group; ##*P* <0.01, ###*P* <0.001 versus the topical treatment group for panels b), c), f), and g).

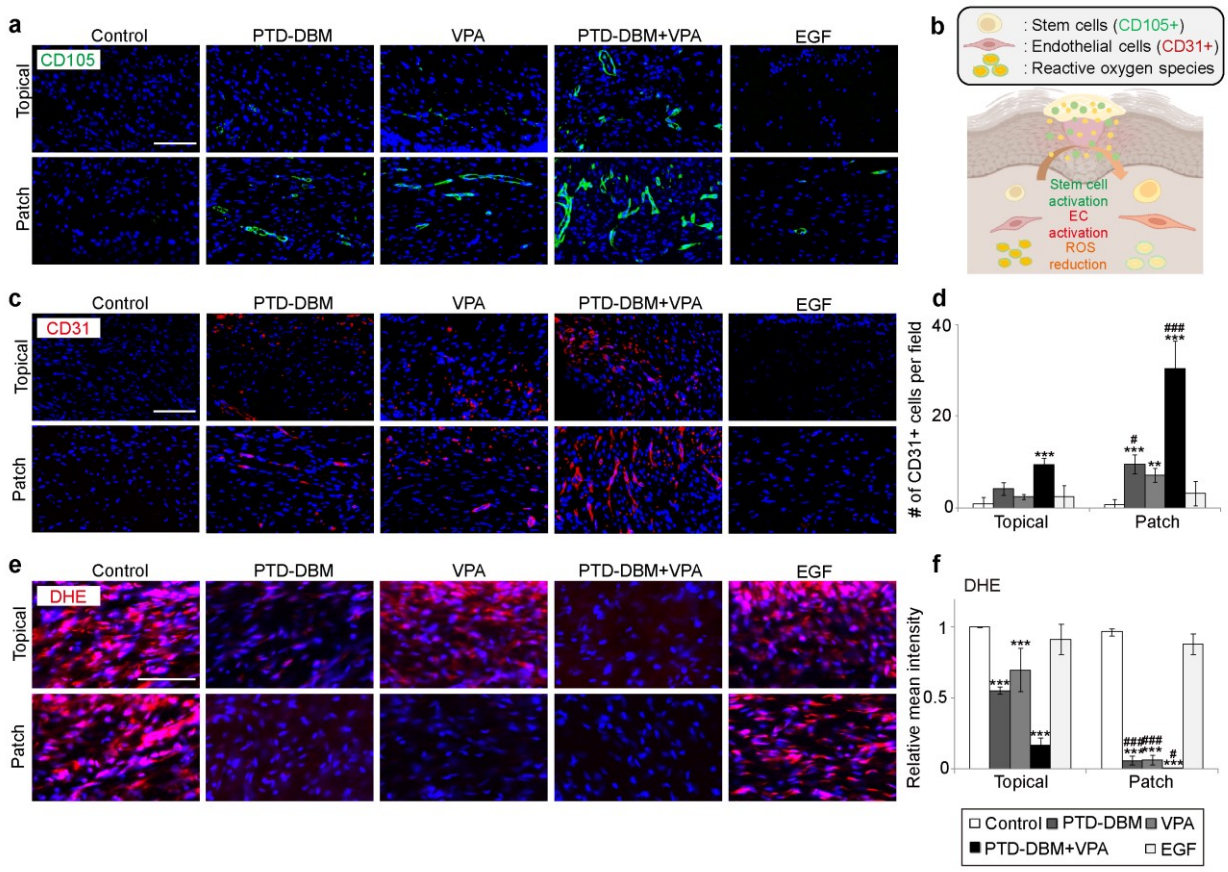

Figure 5. The HA-PG patches with PTD-DBM and/or VPA induced the markers for stem cells and endothelial cells, while reducing ROS in the wounds. a) Immunostaining for CD105 (green) in combination with DAPI staining (blue) in the wound dermis of mice applied topically (upper panel) or via the HA-PG patches (lower panel) with the indicated substances 11 days post-wounding. Scale bar, 100 μm. b) Schematic picture depicting the effects of HA-PG patches with PTD-DBM and VPA on the activation of stem cells and endothelial cells, and levels of ROS. c) Immunohistochemical staining for CD31 (red) with DAPI staining (blue) in the wound dermis. Scale bar, 100 μm. d) Quantification of CD31-positive cells in the wound dermis (n = 5). e) DHE (red) and DAPI nuclei (blue) staining in the wound dermis. Scale bar, 100 μm. f) Quantitative analyses of DHE staining in the wound dermis (n = 5). Significance was determined by the two-way ANOVA test. Data are presented as means ± SD. **P <0.01, ***P <0.001 compared with the control group; #P <0.05, ###P <0.001 compared with the topical treatment group for panels d) and f).

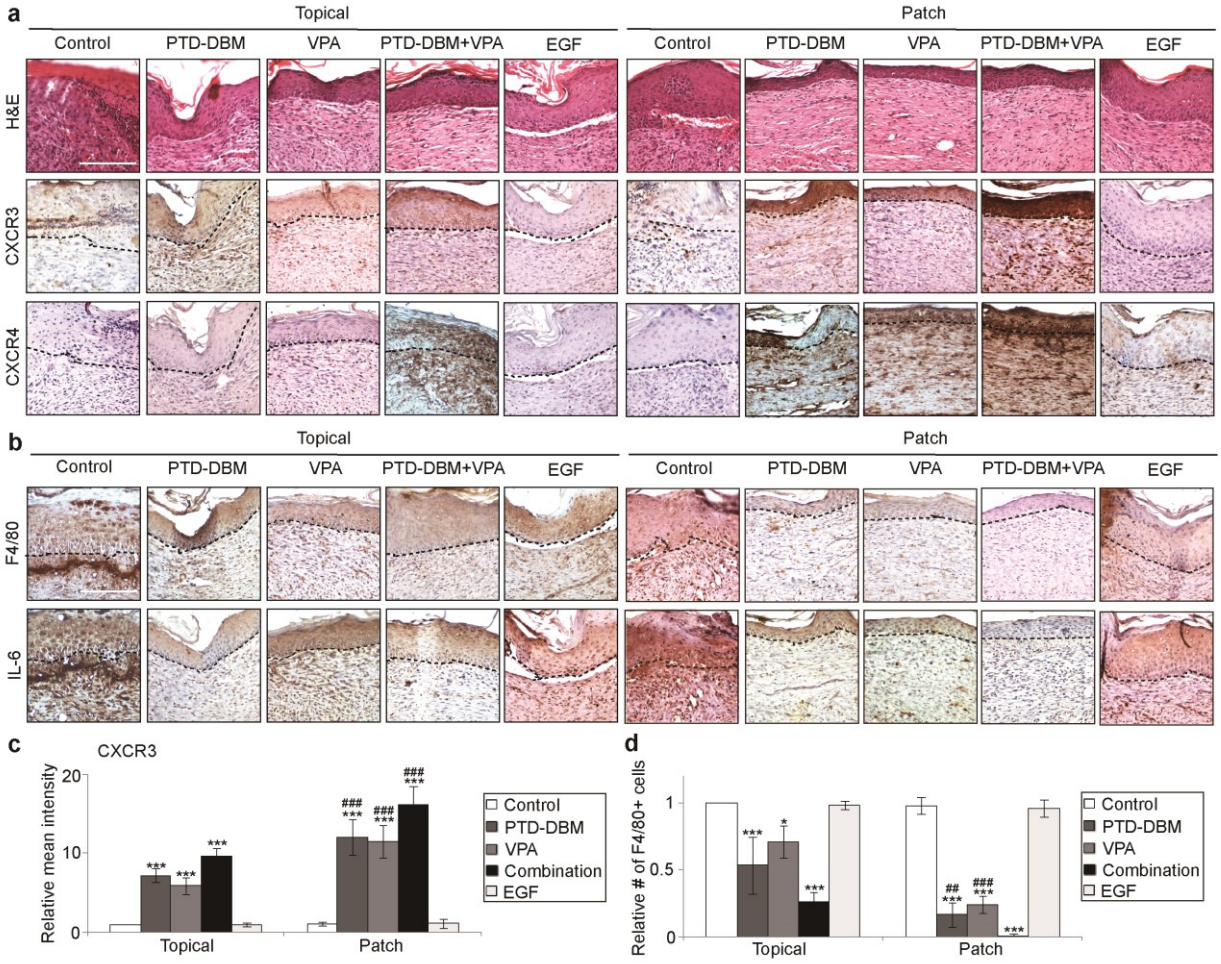

Figure 6. The HA-PG patches with PTD-DBM and/or VPA modulated several chemokines and cytokines. a) H&E (top panel) and DAB staining for CXCR3 (brown, middle panel) and CXCR4 (brown, bottom panel) with Mayer's hematoxylin staining (purple) in the wounds 11 days post-wounding. The dashed lines denote the epidermal-dermal boundaries in the wounds. Scale bar, 100 μm. b) DAB staining for F4/80 (brown, top panel) and IL-6 (brown, bottom panel) with Mayer's hematoxylin staining (purple) in the wounds. The dashed lines indicate dermo-epidermal junctions. Scale bar, 100 μm. c) Mean intensity quantification of CXCR3 in the wounds (n = 5). d) Quantification of F4/80-positive cells in the wounds (n = 5). The two-way ANOVA test was used for statistical analysis. Data are expressed as means ± SD. *P <0.05, ***P <0.001 compared with the control group; ##P <0.01, ###P <0.001 compared with the topical treatment group for panels c) and d).

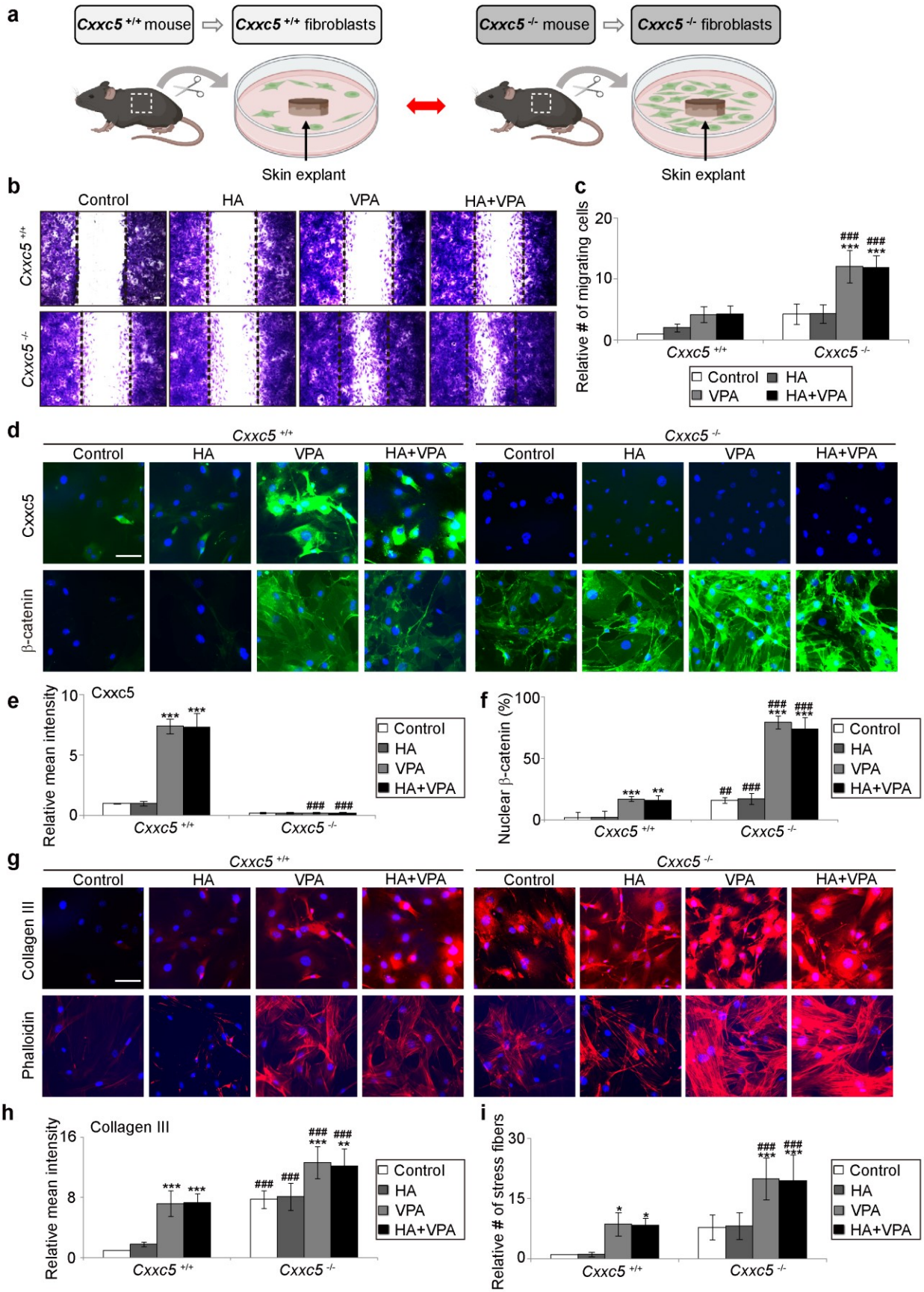

Figure 7. *Cxxc5* knockout mouse fibroblasts recapitulated the regenerative healing phenotype by the HA-PG patches with PTD-DBM and/or VPA. a) Schematic depicting that the *Cxxc5*$^{+/+}$ and *Cxxc5*$^{-/-}$ mouse fibroblasts were derived from skin explants of these mice. b) *In vitro* wound healing assay using *Cxxc5*$^{+/+}$ and *Cxxc5*$^{-/-}$ mouse fibroblasts treated with 1 mg/ml HA and/or 100 μM VPA. The dashed line indicates the width of initially scratched wound. Scale bar, 100 μm. c) Quantification of migrating cell numbers in the *Cxxc5*$^{+/+}$ and *Cxxc5*$^{-/-}$ mouse fibroblasts treated with HA and/or VPA (*n* = 5). d) Immunocytochemical staining for Cxxc5 (green, upper panel) and β-catenin (green, lower panel) in the *Cxxc5*$^{+/+}$ and *Cxxc5*$^{-/-}$ mouse fibroblasts. The Cxxc5 was co-immunostained with Collagen III shown in Figure 7g, and the images of green channel (Cxxc5) were presented merged with the DAPI-stained images (blue). Scale bar, 100 μm. e) Quantitative analyses of immunocytochemical staining for Cxxc5 (*n* = 5). f) Quantification of nuclear β-catenin in the *Cxxc5*$^{+/+}$ and *Cxxc5*$^{-/-}$ mouse fibroblasts (*n* = 5). g) Immunocytochemical staining for Collagen III (red, upper panel) and phalloidin (red, lower panel) in the *Cxxc5*$^{+/+}$ and *Cxxc5*$^{-/-}$ mouse fibroblasts. The Collagen III was co-immunostained with Cxxc5 shown in Figure 7d, and the images of red channel (Collagen III) were presented merged with the DAPI-stained images (blue). Scale bar, 100 μm. h) Mean intensity quantification of Collagen III (*n* = 5). i) Quantification of the number of stress fibers in the *Cxxc5*$^{+/+}$ and *Cxxc5*$^{-/-}$ mouse fibroblasts (*n* = 5). The two-way ANOVA test was used for statistical analysis. Data are presented as means ± SD. **P* <0.05, ***P* <0.01, ****P* <0.001 versus the control group; ##*P* <0.01, ###*P* <0.001 versus the wild-type group for panels c), e), f), h), and i).

ToC contents

The HA-PG patches allow for off-the-shelf availability and dual delivery of PTD-DBM and VPA, and reconstruct the regenerative microenvironment during wound healing. The HA-PG patches with PTD-DBM and VPA critically reduced the markers for differentiated cells and inflammation, but significantly induced the stem cell markers, providing regenerative healing while minimizing scarring.

Keywords: Skin regeneration, Regenerative wound healing, Wnt/β-catenin pathway, Adhesive hydrogel patch, Combination drug therapy

ToC figure